OPTOELECTRONICS LETTERS Vol.20 No.3, 15 March 2024

AWG-based large dynamic range fiber Bragg grating interrogation system*

LI Shufeng[1,2], YUAN Pei[1,2], LI Ke[1,2], LI Ting[1,2], and ZHU Lianqing[1,2]****

1. Key Laboratory of the Ministry of Education for Optoelectronic Measurement Technology and Instrument, Beijing Information Science & Technology University, Beijing 100192, China

2. Beijing Laboratory of Optical Fiber Sensing and System, Beijing Information Science & Technology University, Beijing 100016, China

(Received 26 June 2023; Revised 6 August 2023)

Arrayed waveguide gratings (AWGs) are extensively employed in fiber Bragg grating (FBG) interrogation systems due to their compact size, lightweight nature, and excellent interrogation performance. The resolution and total measurement range of AWG-based FBG interrogation systems are constrained by the output properties of AWG. We proposed an AWG-based large dynamic range interrogation system. The temperature dependence of AWG is exploited to achieve continuous interrogation. The test results show that the interrogation system has a dynamic range of 28.67 nm, an interrogation accuracy better than 25 pm, and a wavelength resolution of 6 pm.

Document code: A **Article ID:** 1673-1905(2024)03-0129-6

DOI https://doi.org/10.1007/s11801-024-3115-4

In recent years, fiber Bragg grating interrogator (FBGI) has gained widespread adoption for structural health monitoring of infrastructure, encompassing applications like deformation and settlement monitoring of bridges and tunnels, load measurement of wind turbines, and icing measurement, among others[1-4]. The central wavelength of the light reflected by the FBG undergoes a shift in response to changes in the surrounding environment. This subtle shift is detected by the data processing unit, which subsequently analyzes, processes, and interrogates the dynamic signal. The advancement of integrated optical technology has led to the emergence of numerous highly integrated and miniaturized FBGIs. Among these, the arrayed waveguide gratings (AWGs) based FBGI has garnered significant attention due to its superior interrogation performance[5-14].

The dynamic range of interrogation serves as a crucial performance indicator for FBGI. Nevertheless, constrained by the spectral characteristics of AWG, a large dynamic range tends to reduce the resolution of interrogation[15,16]. In Refs.[17] and [18], the dynamic range of the interrogation was expanded by adding a multimode interference (MMI) coupler at the input of the AWG to increase spectral overlap. The reported dynamic ranges were 10 nm and 28 nm, respectively. However, the MMI coupler increases the overall loss of the device, thereby placing higher demands on the capacity of the photodetector (PD).

In this paper, we present an analysis of the temperature dependence of AWG and discuss the principles of an AWG-based interrogation system. We proposed an interrogation system for large dynamic range FBG based on AWG. The system leverages the temperature properties of AWG to enhance its spectral overlap. By adopting this approach, the system can expand its interrogation range without compromising the wavelength resolution.

AWG on silicon-based planar lightwave circuits (PLCs) has demonstrated excellent interrogation performance[19]. However, the large size of the PLC-AWG devices hinders the integration of photonic-integrated devices. Moreover, the high thermal stability of PLC-AWG renders it unsuitable for our proposed interrogation system, which relies on modulating the chip temperature to achieve continuous interrogation. The significant refractive index difference in the silicon-on-insulator (SOI) material results in shorter decoupling distances between waveguides and smaller bending radius for curved waveguides, both of which significantly reduce the footprint of the AWG. Additionally, the SOI waveguide-based modulators exhibit rapid response rates, with a thermal response time of better than 50 ms. This response time is ample for interrogation systems. We designed a 10-channel SOI-based AWG, and its structural diagram is illustrated in Fig.1. The AWG utilizes a 220-nm-thick rib waveguide with a rib width of 500 nm and a rib height of 150 nm. The arrayed waveguide spacing is d=1 μm, and the input/output waveguide spacing is Δx=1.5 μm. Detailed design

---

* This work has been supported by the National Natural Science Foundation of China (No.62205030), and the R&D Program of Beijing Municipal Education Commission (No.KM202211232019).

** E-mails: yuanpei@bistu.edu.cn; lqzhu_bistu@sina.com parameters can be found in Tab.1.

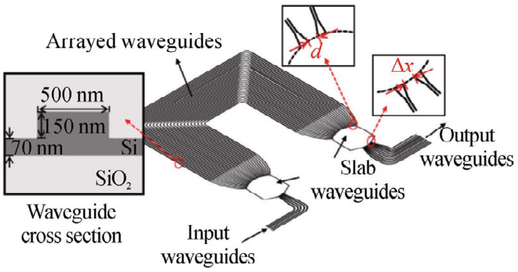

Fig.1 Structure diagram of the SOI-based AWG

Tab.1 Parameters of the AWG

Parameter	Value
Number of channels	2 in, 10 out
Number of arrayed waveguides	55
Channel spacing ($\Delta\lambda$)	3.2 nm
Diffraction order (m)	20
Diameter of Rowland circle (R)	49.278 μm
Path difference of arrayed waveguides (ΔL)	11.351 μm

Neglecting the transmission loss, the output spectrum of the AWG can be represented by a transfer function as shown in

$$T = \left| \sum_{j=-M}^{M} \left[\rho_{\mathrm{g}}(j,0)\right]^2 \times \exp \mathrm{i}\frac{2\pi}{\lambda}\{j[n_{\mathrm{s}} d\left(\theta_{\mathrm{i}}+\theta_{\mathrm{o}}\right)+ \left(n_{cj}\Delta L_j + \phi(j)\right)]\} \right|^2, \tag{1}$$

where M is half the number of arrayed waveguides, $\rho_{\mathrm{g}}(j, 0)$ is the Gaussian mode field distribution of the jth arrayed waveguide, n_{s} is the effective refractive index of the slab waveguide, n_{c} is the effective refractive index of the arrayed waveguide, $\theta_{\mathrm{i}}=\Delta x_{\mathrm{i}}/R$, $\theta_{\mathrm{o}}=\Delta x_{\mathrm{o}}/R$, and $\phi(j)$ is the random fluctuation of $n_{cj}\Delta L_j$. We utilized the transfer function to simulate the output spectrum of the AWG, and the results are depicted in Fig.2. The AWG output spectrum spans from 1 523 nm to 1 556 nm. Each channel's output spectrum follows a Gaussian distribution, with a channel spacing of 3.2 nm and a 3 dB bandwidth of approximately 2 nm.

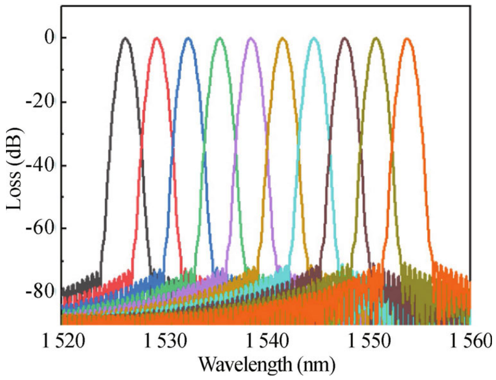

Fig.2 Simulated transmission spectra of AWG

The AWG chip is fabricated with a 180 nm process line by United Micro-Electronics Center (CUMEC) Co., Ltd in China. The fabrication process is depicted in Fig.3. The first step involves cleaning the substrate surface. Next, a uniform layer of photoresist is applied to the substrate, followed by exposure to the substrate using deep ultraviolet lithography (DUVL) to create the desired pattern. The silicon waveguide is then etched using the inductively coupled plasma (ICP) technique. Subsequently, clean the photoresist. Finally, a protective silica layer is formed using plasma enhanced-chemical vapor deposition (PECVD). The footprint of the AWG is 488 μm×583 μm.

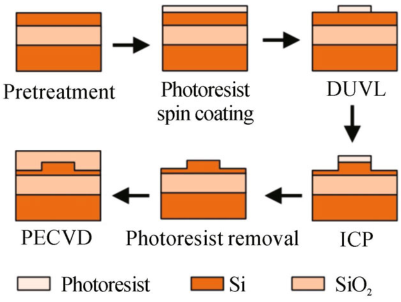

Fig.3 Fabrication process of the AWG

We tested the spectrum of the AWG using the device in Fig.4. The AWG is placed on a temperature console, which is controlled by a temperature control system to maintain the temperature at 30 °C. A single-mode fiber (SMF), controlled by 6-axis adjustment platform, vertically couples light from the amplified spontaneous emission (ASE) light source into the AWG. The output of the AWG is connected to an optical spectrum analyzer (OSA) and an optical power meter (OPM) through a splitter, respectively. The spectrum of AWG at 30 °C is shown in Fig.5. It can be seen that the insertion loss is about 2.5—6.5 dB, the crosstalk is about −20 dB, and the half-peak bandwidth is about 2.5 nm.

Eq.(2) is the grating equation satisfied by the input and output light of AWG

$$n_{\mathrm{s}} d \sin\theta_{\mathrm{in}} + n_{\mathrm{c}}\Delta L + n_{\mathrm{s}} d \sin\theta_{\mathrm{out}} = m\lambda. \tag{2}$$

Due to thermo-optical effects, temperature changes will cause a drift in the spectrum of the AWG. Eq.(2) takes the derivative of temperature to obtain the AWG dependence on the temperature equation, as shown in

$$\mathrm{d}\frac{\mathrm{d}n_{\mathrm{s}}}{\mathrm{d}T}(\sin\theta_{\mathrm{in}} + \sin\theta_{\mathrm{out}}) + \frac{\mathrm{d}n_{\mathrm{c}}}{\mathrm{d}T}\Delta L + n_{\mathrm{c}}\frac{\mathrm{d}\Delta L}{\mathrm{d}T} = m\frac{\mathrm{d}\lambda}{\mathrm{d}T}. \tag{3}$$

The wavelength drift rate of the central wavelength with temperature is shown as

$$\frac{\mathrm{d}\lambda_{\mathrm{c}}}{\mathrm{d}T} = \frac{\lambda_{\mathrm{c}}}{n_{\mathrm{c}}}\left(\frac{\mathrm{d}n_{\mathrm{c}}}{\mathrm{d}T} + n_{\mathrm{c}}\alpha_{\mathrm{sub}}\right), \tag{4}$$

where α_{sub} is the coefficient of thermal expansion (CTE) of the substrate material. The CTE of silicon substrates is approximately 2.63×10^{-6}/°C. The temperature-dependent central wavelength shift (TD-CWS) can be expressed as

$$\Delta\lambda = \lambda_0' - \lambda_0 = \frac{\lambda_0}{n_{c0}}\left\{n_c \exp\left[\alpha_{sub}\left(T - T_0\right)\right] - n_{c0}\right\}, \qquad (5)$$

where λ'_0 and n_{c0} are the wavelength and the effective index of the arrayed waveguides at the temperature of T_0, respectively.

At 1 550 nm, the refractive index is 3.475 7 for Si and 1.444 for SiO_2. The thermal optical coefficient is 1.8×10^{-4}/°C for Si and 1×10^{-5}/°C for SiO_2. According to the above equations, the temperature drift of the central wavelength of the SOI-based AWG is calculated to be approximately 0.117 nm/°C.

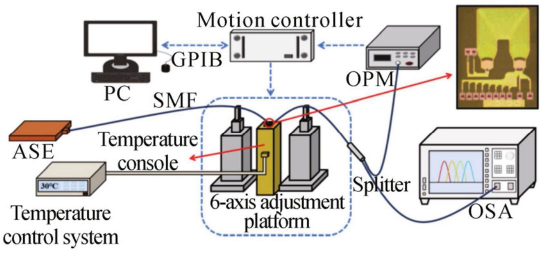

Fig.4 Testing system for the spectrum measurement of the AWG

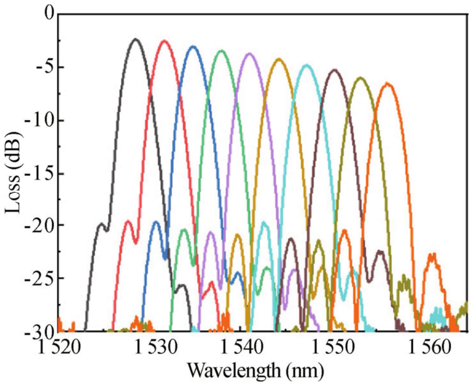

Fig.5 Spectra of the AWG at 30 °C

We conducted spectrum testing of the AWG at various temperatures using the setup illustrated in Fig.4. The temperature control system regulated the temperature of the temperature console over the range from 25 °C to 80 °C. Fig.6(a) illustrates the spectra of AWG's channel 5 at different temperatures. The intensity of the center wavelength exhibits slight variation at different temperatures, attributed to the mechanical vibrations of the test equipment. Fig.6(b) depicts the relationship between the central wavelength of AWG's channel 5 and temperature. It can be concluded that the spectrum of AWG drifts about 0.077 nm/°C. The observed temperature drift in the test is lower than the calculated value due to the thermal convection of the air, causing the chip temperature to fall below the temperature set by the temperature console.

Fig.7 shows the wavelength distribution of AWG and FBG. The extent of overlap between the FBG reflection spectrum and the AWG transmission spectrum governs the optical power magnitude of the two adjacent output channels of the AWG. The relationship between the logarithm of AWG's adjacent output channel optical power ratio and the central wavelength of FBG can be calculated and expressed as

$$\ln\left(\frac{P_{i+1}}{P_i}\right) = \frac{8(\ln 2)\Delta\lambda}{\Delta\lambda_{FBG}^2 + \Delta\lambda_i^2}\lambda_{FBG} - \frac{4(\ln 2)\left(\lambda_{i+1}^2 + \lambda_i^2\right)}{\Delta\lambda_{FBG}^2 + \Delta\lambda_i^2}, \qquad (6)$$

where P_i and P_{i+1} are the output powers of the AWG's channels i and i+1. $\Delta\lambda$ is the offset of the central wavelength, λ_i, λ_{i+1} and λ_{FBG} are the center wavelengths of AWG's channel i, i+1 and FBG, respectively. $\Delta\lambda_i$ and $\Delta\lambda_{FBG}$ are the half-peak bandwidths of AWG and FBG spectra. The central wavelength of the FBG can be successfully interrogated using Eq.(6).

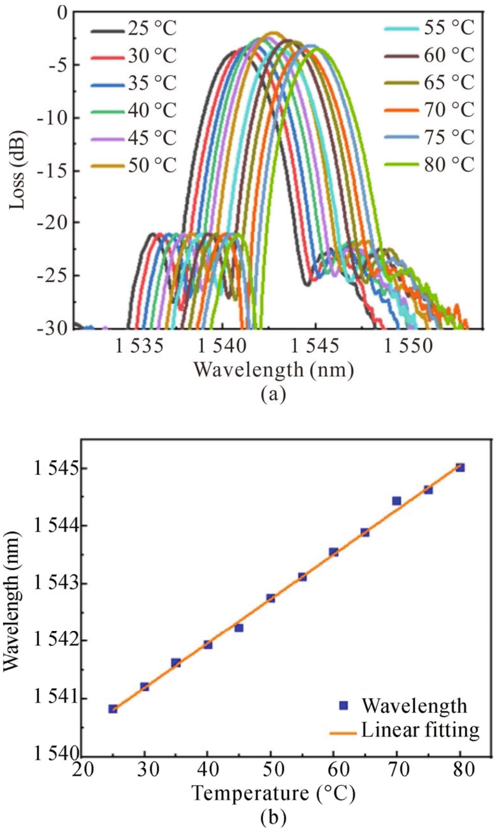

Fig.6 (a) Spectra of AWG's channel 5 at different temperatures; (b) Relationship between the central wavelength of AWG's channel 5 and temperature

Fig.8 shows a schematic diagram of the interrogation principle. At a given temperature T, the dynamic range of the interrogation is λ_R. Upon a temperature change to T', the spectral drift becomes $\Delta\lambda$, and the new interrogation dynamic range is λ'_R. However, when the FBG's reflectance spectrum falls within λ'_R, the interrogation range at T is exceeded, rendering the FBG wavelength cannot be interrogated at this point. By changing the temperature of the AWG to T', the interrogation range shifts to λ'_R, thereby successfully interrogating the reflected wavelength of the FBG. It can be seen that the dynamic range of the interrogation is extended from λ_R to λ''_R ($\lambda''_R=\lambda_R+\lambda'_R$) by temperature change.

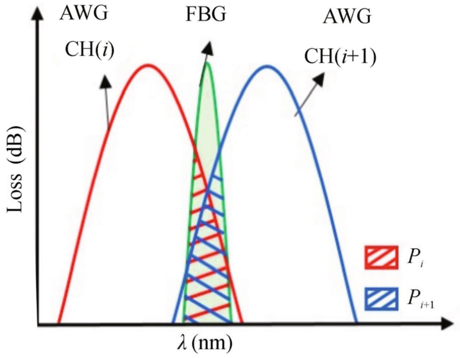

Fig.7 Schematic diagram of the relative strength interrogation

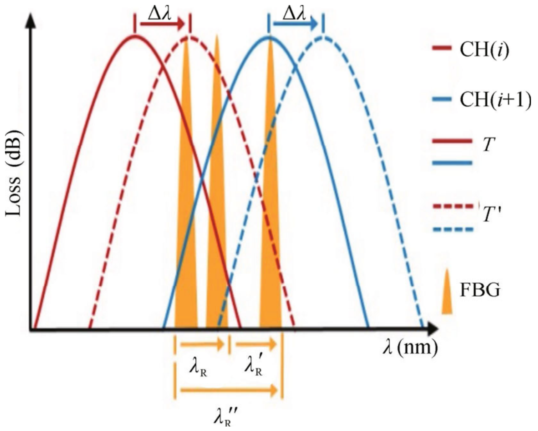

Fig.8 Schematic diagram of the interrogation system principle

Based on the above principle, we designed an interrogation system, as shown in Fig.9. ASE provides a broad-spectrum light source for the system. Multiple FBGs are connected in series to access the system. The total number of FBGs in the system is denoted by n, where $n \le N/2$ (N is the number of AWG output channels). The narrowband light reflected from the FBG passes through the circulator into the AWG. The optical signal from the AWG is converted into an electrical signal by the PD and fed into the subsequent data processing circuit. The temperature control circuit modulates the AWG chip temperature, inducing a wavelength drift in the output. Within a single cycle, the temperature control circuit maintains the chip temperature at 30 °C, 40 °C, 50 °C, 60 °C, and 70 °C, while the microcomputer collects data from each channel of the AWG at different temperatures. After one cycle of scanning, the channels that have responded and their corresponding temperature are identified. Using this information, the interrogation can be completed.

We conducted interrogation tests using the SOI-based 10-channel AWG chip mentioned above to evaluate the performance of the interrogation system. We employed the same experimental setup as shown in Fig.4 but substituted a tunable laser for the ASE. The reflected light from the FBG sensor is replaced by a single narrow-band light output from the tunable laser. The OPM is used to continuously track the optical power of the two adjacent AWG's output channels. The temperature console was used to regulate the AWG's temperature at 30 °C, 40 °C, 50 °C, 60 °C, and 70 °C, allowing us to test the interrogation performance at each of these five temperatures.

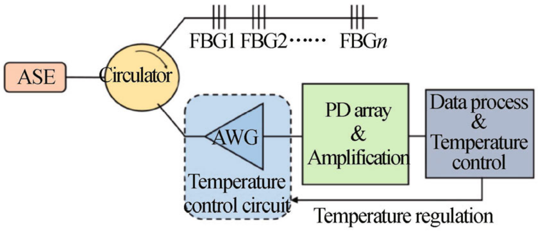

Fig.9 AWG-based large dynamic range FBG interrogation system

Fig.10 shows the results of the interrogation experiments. The interrogation ranges for CH1 & CH2 at the five temperatures are continuous, and this range also connects seamlessly with the interrogation range for CH2 & CH3 at 30 °C. Thus, the system allows for continuous interrogation. The interrogation range of CH10 & CH11 at 70 °C spans from 1 557.60 nm to 1 558.40 nm. Consequently, the total interrogation range of the system is from 1 529.73 nm to 1 558.40 nm, achieving continuous interrogation over a range of 28.67 nm. The interrogation function is obtained through linear fitting of the experimental data. The central wavelength of FBG interrogated using CH1 & CH2 is given by

$$\lambda_{\mathrm{FBG}}=\begin{cases}0.354\,7\dfrac{P_2}{P_1}+1\,530.113\,7 & (T=30\ ^\circ\mathrm{C})\\ 0.365\,0\dfrac{P_2}{P_1}+1\,530.847\,1 & (T=40\ ^\circ\mathrm{C})\\ 0.374\,1\dfrac{P_2}{P_1}+1\,531.593\,3 & (T=50\ ^\circ\mathrm{C})\\ 0.366\,9\dfrac{P_2}{P_1}+1\,532.423\,7 & (T=60\ ^\circ\mathrm{C})\\ 0.374\,8\dfrac{P_2}{P_1}+1\,533.172\,3 & (T=70\ ^\circ\mathrm{C})\end{cases}. \tag{7}$$

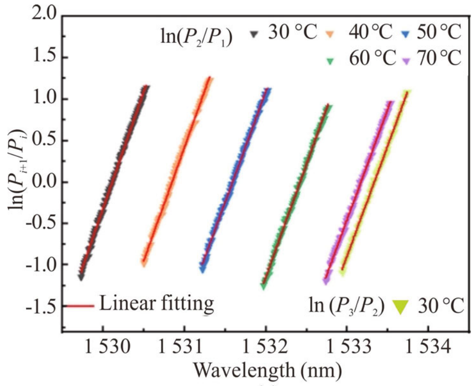

(a)

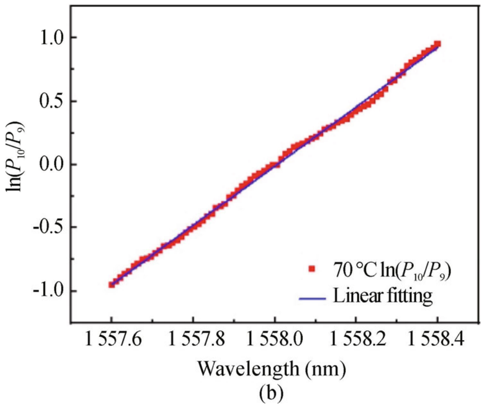

(b)

Fig.10 (a) Interrogation results for CH1 & CH2 and CH2 & CH3 at different temperatures; (b) Interrogation results for CH9 & CH10 at 70 °C

The root mean square error (RMSE) between the actual test data and the fitted function is the interrogation accuracy. The accuracy for each data set is presented in Tab.2. This interrogation system has a wavelength interrogation accuracy of better than 25 pm.

Tab.2 Interrogation performance

Channel	T	Dynamic range	Accuracy
1 & 2	30 °C	1 529.73—1 530.53 nm	20.12 pm
1 & 2	40 °C	1 530.50—1 531.31 nm	22.56 pm
1 & 2	50 °C	1 531.22—1 532.02 nm	20.79 pm
1 & 2	60 °C	1 531.97—1 532.77 nm	24.07 pm
1 & 2	70 °C	1 532.74—1 533.54 nm	19.32 pm
2 & 3	30 °C	1 532.94—1 533.74 nm	19.51 pm
9 & 10	70 °C	1 557.60—1 558.40 nm	23.23 pm

We also tested the wavelength resolution of the system. The wavelength scan range of the tunable laser was set from 1 530.1 nm to 1 530.2 nm, with a scan step of 1 pm. At each step, the optical power was recorded using an OPM. The results are shown in Fig.11, where ln(P_2/P_1) changes significantly when the wavelength changes by 6 pm. Consequently, the resolution of the interrogation system is determined to be 6 pm.

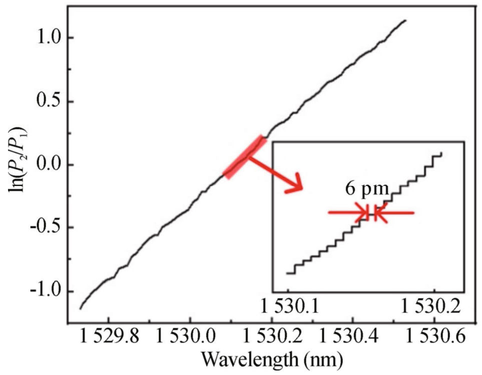

Fig.11 Resolution test result of the interrogation system

Based on the above test results, we compared the interrogation performance of our designed AWG chip in two interrogation systems. System A represents the interrogation system at a single temperature (30 °C), and the corresponding interrogation results have been presented in Tab.2. System B is the large dynamic range interrogation system designed in this paper. The results are shown in Tab.3. As observed, our designed interrogation system exhibits a broader dynamic range and enables continuous interrogation.

Tab.3 Comparison of interrogation performance

	Dynamic range	Accuracy	Resolution	Continuous interrogation
A	0.8 nm	< 21 pm	6 pm	No
B	28.67 nm	< 25 pm	6 pm	Yes

We ran numerous sets of repeated tests to confirm the stability of the system since the optical waveguide coupling process is easily impacted by the disruption of the external environment. The outcomes of the experiment are displayed in Fig.12. The findings demonstrate that the interrogation system has good stability because the accuracy of the interrogation system is consistently in the range from 20 pm to 25 pm and the resolution is consistently in the range from 4 pm to 6 pm.

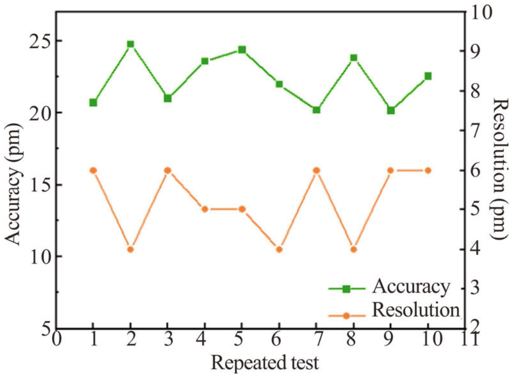

Fig.12 Stability test results of the interrogation system

The AWG designed in this paper has a large channel spacing, which results in a lower spectral slope. According to Eq.(6), the slope of the interrogation function is constrained by the spectrum, which in turn affects the resolution of the interrogation system. And the design of the AWG has a small free spectral range (FSR), which constrains the interrogation range. In subsequent studies, we can achieve better interrogation performance by reducing the channel spacing of the AWG and increasing the FSR of the AWG. To mitigate the mutual thermal influence between the AWG and the FBG, the AWG thermal conditioning module can be encapsulated with an insulating material. This encapsulation effectively isolates the AWG from external temperature variations, thus minimizing their impact on the FBG. Additionally, optimizing the system layout by increasing the spatial separation between the AWG and FBG modules can further reduce thermal conduction between them, achieving better decoupling of their temperature responses.

In summary, we proposed an AWG-based large dynamic range FBG interrogation system. Unlike the conventional FBG interrogation technique, this study utilizes the AWG as the core device of the interrogation system. There are no mechanical moving parts inside the AWG, which results in a faster interrogation rate. We also creatively utilized the thermo-optic effect of SOI materials to make the wavelength of AWG tunable, thus increasing the spectral overlap of the device. This broad spectral overlap greatly enhances the system's interrogation range while maintaining high interrogation accuracy and wavelength resolution, resulting in high-performance, wide-range, continuous interrogation. The wavelength interrogation results are also improved by our interrogation method, which employs signals from two channels to interrogate an FBG. We tested the performance of this interrogation system using an SOI-based 10-channel AWG. The results show that the system has a large dynamic range of 28.67 nm, an interrogation accuracy of better than 25 pm, and a wavelength resolution of 6 pm. This study introduces a novel interrogation solution for a miniaturized FBG continuous interrogation system. The system exhibits remarkable versatility and can effectively interrogate signals, such as pressure, strain, and vibration.

Ethics declarations

Conflicts of interest

The authors declare no conflict of interest.

References

[1] WANG T, LIU K, JIANG J, et al. Temperature-insensitive refractive index sensor based on tilted moire FBG with high resolution[J]. Optics express, 2017, 25(13): 14900-14909.

[2] CULSHAW B, KERSEY A. Fiber-optic sensing: a historical perspective[J]. Journal of lightwave technology, 2008, 26(9): 1064-1078.

[3] LEAL-JUNIOR A G, DIAZ C A R, AVELLAR L M, et al. Polymer optical fiber sensors in healthcare applications: a comprehensive review[J]. Sensors (Basel), 2019, 19(14).

[4] LI K, DONG M L, YUAN P, et al. Review of fiber Bragg grating interrogation techniques based on array waveguide gratings[J]. Acta physica sinica, 2022, 71(9): 094207.

[5] LI H, GAO W, LI E, et al. Investigation of ultrasmall 1×N AWG for SOI-based AWG demodulation integration microsystem[J]. IEEE photonics journal, 2015, 7(6): 1-7.

[6] LI H, MA X, CUI B, et al. Chip-scale demonstration of hybrid III-V/silicon photonic integration for an FBG interrogator[J]. Optica, 2017, 4(7): 692-700.

[7] LI K, YUAN P, LU L, et al. PLC-based arrayed waveguide grating design for fiber Bragg grating interrogation system[J]. Nanomaterials (Basel), 2022, 12(17): 2938.

[8] LI S, YUAN P, LI T, et al. SOI-based 15-channel arrayed waveguide grating design for fiber Bragg grating interrogator[J]. Photonics and nanostructures-fundamentals and applications, 2023, 53.

[9] MARIN Y E, NANNIPIERI T, OTON C J, et al. Current status and future trends of photonic-integrated FBG interrogators[J]. Journal of lightwave technology, 2018, 36(4): 946-953.

[10] MENDOZA E A, ESTERKIN Y, KEMPEN C, et al. Multi-channel monolithic integrated optic fiber Bragg grating sensor interrogator[J]. Photonic sensors, 2011, 1(3): 281-288.

[11] SU H, HUANG X G. A novel fiber Bragg grating interrogating sensor system based on AWG demultiplexing [J]. Optics communications, 2007, 275(1): 196-200.

[12] VIVIEN L, HONKANEN S, PAVESI L, et al. Design, integration, and testing of a compact FBG interrogator, based on an AWG spectrometer[J]. Proceedings of SPIE, 2014, 9133: 91330D.

[13] WANG H, TAO C, GAO X, et al. Detection of dynamic strain using an SOA-fiber ring laser and an arrayed waveguide grating demodulator[J]. Optoelectronics letters, 2022, 18(6): 331-337.

[14] WENG S, YUAN P, ZHUANG W, et al. SOI-based multi-channel AWG with fiber Bragg grating sensing interrogation system[J]. Photonics, 2021, 8(6): 214.

[15] JI S, LI K, YUAN P, et al. Design and fabrication of AWG with large bandwidth applied in FBG interrogation system[J]. Optics & laser technology, 2022, 149: 107372.

[16] YUAN P, WENG S, JI S, et al. Performance analysis of fiber Bragg grating sensor interrogators based on arrayed waveguide gratings[J]. Optical engineering, 2021, 60(06): 066101.

[17] PUSTAKHOD D, KLEIJN E, WILLIAMS K, et al. High-resolution AWG-based fiber Bragg grating interrogator[J]. IEEE photonics technology letters, 2016, 28(20): 2203-2206.

[18] WENG S, YUAN P, LU L, et al. SOI-based arrayed waveguide grating with extended dynamic range for fiber Bragg grating interrogator[J]. Optical fiber technology, 2022, 68(8): 102815.

[19] MENDOZA J P, KEMPEN C, SUN S, et al. Fully integrated miniature multi-point fiber Bragg grating sensor interrogator (FBG-transceiver) system for applications where size, weight, and power are critical for operation[C]//6th European Workshop on Structural Health Monitoring (EWSHM 2012), July 3-6, 2012, Dresden, Germany. Berlin, Heidelberg: Springer-Verlag, 2012.